Journal of the Physical Society of Japan
Vol. 66, No. 3, March, 1997, pp. 818-826

Dynamical Susceptibility in Ferromagnetic Metal of CoS_2 - Inelastic Magnetic Neutron Scattering -

Haruhiro HIRAKA, Yasuo ENDOH and Kazuyoshi YAMADA

Department of Physics, Graduate School of Science, Tohoku University, Aramaki Aza Aoba, Aoba-ku, Sendai 980-77

(Received October 28, 1996)

Inelastic neutron scattering experiments from a ferromagnetic metal of CoS_2 have been performed in a wide (q,ω) space and a wide temperature range across the Curie temperature, T_C. Magnetic excitations in a small q region are well characterized to be spin-waves below T_C. The sharp response of the spin-wave scattering suddenly broadens at $q > 0.27$ Å^{-1} and $\omega > 8$ meV. The paramagnetic fluctuations above T_C are centered at $\omega = 0$ meV, which could be analyzed by a double Lorentzian form in q and ω. The line width Γ satisfies the dynamical scaling hypothesis; $\Gamma = A_0 q^{2.5} f(\kappa_1/q)$. The dynamical feature in both below and above T_C indicates that CoS_2 is regarded as a typical itinerant ferromagnet.

KEYWORDS: CoS_2, inelastic neutron scattering, spin-wave excitations, Stoner excitations, dynamical scaling law

§1. Introduction

Transition metal disulfides, MS_2 with M = Fe, Co, Ni, Cu and Zn of a common pyrite structure exhibit a variety in electric conductivity and magnetism.[1,2] For instance, NiS_2 is an antiferromagnetic Mott insulator and the substitution of Se to S gives rise to the insulator-metal transition.[3] CuS_2 becomes a superconductor[4] and $Co(S_xSe_{1-x})_2$ is known to show the metamagnetic transition under high magnetic field.[5,6] This interesting feature was well explained by Ogawa *et al.*,[7,8] who worked out the band filling in the narrow d band as well as the strength of electron correlation by changing the transition element M in this system.

According to the tight binding band calculations for CoS_2,[9] the d band splits to two sub-bands consisting of a lower t_{2g} and a higher e_g symmetry and the paramagnetic Fermi level sits on the middle of the e_g band with a quarter filled electron occupancy. The theoretical band structure was confirmed by X-ray photoemission spectroscopy[10] as well as reflectivity and absorption spectra.[11] Then the electron correlation brings the ferromagnetic long range order with the Curie temperature, T_C, of about 120 K. Note that the strength of electron correlation was assigned to be intermediate considering the relatively low T_C, with supplemental experimental facts of the fractional magnetic moment of $\mu_s(0.84 \sim 0.90\mu_B)$,[1,2] the smaller coefficient of the electronic specific heat[12,13] and correspondingly the small magnetic entropy.[12,14] The same assignment was made from a theoretical side by fitting the calculated magnetic susceptibility based on the self-consistent renormalization (SCR) theory to the experimental data of the static magnetic susceptibility of CoS_2.[15-17] Nevertheless, these facts are favorable to inelastic neutron scattering experiments investigating spin dynamics, since the energy scale of thermal neutrons accomodates to the dominant part of spin dynamics in CoS_2.

The previous work on the static critical properties of CoS_2 by Hiraka and Endoh[18] revealed that CoS_2 can be regarded as a three dimensional isotropic ferromagnet with a saturated moment, although the critical exponents deviate from those in an ideal Heisenberg ferromagnet. The fact of the true second order phase transition was confirmed in the previous experiments, since the static scaling laws are completely satisfied. Therefore, the deviation was revealed to reflect only the tricriticality; in other words, the phase transition point on the second order phase transition line locates at the vicinity of a tricritical point. In fact, the first order phase transition was also observed by the recent experiments either at high pressure applied on CoS_2 or from $Co(S_xSe_{1-x})_2$.[19] The authors concluded that the effect of the itinerancy or the band character on the magnetic phase transition in CoS_2 remains as a subtle subject, although there exist several papers speculating such effects.[20,21]

In the present study, we elucidated the dynamical susceptibility in a wide (q,ω) as well as temperature range by using inelastic neutron scattering technique. The inelastic neutron scattering experiment made by Iizumi *et al.*[22] is only a reliable report as far as we know, in which low-energy magnetic excitations up to 8 meV give an isotropic quadratic dispersion with respect to q at low temperatures. As we know that the magnetic moment in CoS_2 is relatively small and also Co itself is a neutron absorber, the inelastic neutron scattering experiments are no easy task. Therefore, we could make a great effort for the sample preparation to overcome these problems.

Since we have accumulated the experimental data on the spin dynamics or $S(q,\omega)$ of various ferromagnets ranging from the localized moment system, such as EuO and Pd_2MnSn to the itinerant electron system, such as Fe, Ni and MnSi. Therefore, we can make a quantitative comparison of observed data of CoS_2 with these results from other ferromagnets just mentioned above and discuss the issue of itinerant characteristics in CoS_2.

The format of this paper is following. In §2, the neutron magnetic scattering cross-sections are presented as a matter of convenience to the readers. The experimental procedure including sample preparation will be described in §3. The experimental results will be presented in §4, followed by the discussion in §5. Finally, §6 is devoted to the conclusion remarks.

§2. Neutron Magnetic Cross-Sections

In general, the neutron magnetic scattering cross-section is proportional to the imaginary part of the dynamical magnetic susceptibility $\chi(\boldsymbol{Q},\omega)$;[23,24]

$$\frac{\mathrm{d}^2\sigma}{\mathrm{d}\Omega\mathrm{d}\omega} = \frac{k_\mathrm{f}}{k_\mathrm{i}} S(\boldsymbol{Q},\omega), \tag{2.1}$$

$$S(\boldsymbol{Q},\omega) \propto f_\mathrm{m}(\boldsymbol{Q})^2 \frac{1}{1-\exp(-\hbar\omega/k_\mathrm{B}T)} \mathrm{Im}\chi(\boldsymbol{Q},\omega), \tag{2.2}$$

with the conventional notations.

2.1 $T < T_C$

The following spin-wave formula which holds in a ferromagnet is employed,

$$\left(\frac{\mathrm{d}^2\sigma}{\mathrm{d}\Omega\mathrm{d}\omega}\right)_\mathrm{sw} = C_\mathrm{sw}\frac{k_\mathrm{f}}{k_\mathrm{i}} f_\mathrm{m}(\boldsymbol{Q})^2 \frac{1}{1-\exp(-\hbar\omega/k_\mathrm{B}T)} \times \frac{\Gamma}{(\hbar\omega - Dq^2)^2 + \Gamma^2}, \tag{2.3}$$

where D stands for the spin-wave stiffness constant, Γ the half width at half maximum and C_sw the scale factor. $\hbar/\Gamma$ corresponds to the finite life-time of spin-wave excitaions. q is the momentum transfer measured from a reciprocal lattice point.

To examine the mechanism of magnetic excitaions in CoS_2, in other words, to distinguish the magnetic excitations coming from the localized spins or the itinerant electrons, we analyze the experimental data on the basis of eq. (2.3) with the convolution of instrumental resolution effects. Then, we discuss the the dispersion curve, C_sw and Γ.

2.2 $T > T_C$

A series of paramagnetic scattering experiments performed systematically at the Brookhaven National Laboratory in the middle of 1980' indicated that a simple scattering function,

$$S(\boldsymbol{Q},\omega) = f_\mathrm{m}(\boldsymbol{Q})^2 \frac{\hbar\omega/k_\mathrm{B}T}{1-\exp(-\hbar\omega/k_\mathrm{B}T)} 2k_\mathrm{B}T\chi(0) \times \frac{\kappa_1^2}{\kappa_1^2+q^2}\frac{1}{\pi}\frac{\Gamma}{\Gamma^2+(\hbar\omega)^2}, \tag{2.4}$$

describes successfully the essential features of the observed paramagnetic scattering from cubic ferromagnets such as Fe,[25] Ni,[26] EuO,[27] Pd_2MnSn[28] and MnSi.[29,30] Here, $\chi(0)$ is the static susceptibility and κ_1 the inverse correlation length. The dynamical scaling law above T_C predicts the linewidth of

$$\Gamma = A_0 q^{2.5} f(\kappa_1/q), \tag{2.5}$$

where $f(x)$ is a scaling function being unity as $x \to 0$ (critical regime) and proportional to $x^{1/2}$ as $x \to \infty$ (hydrodynamic regime).[31]

Accordingly, we use the following cross-section for the paramagnetic scattering,

$$\left(\frac{\mathrm{d}^2\sigma}{\mathrm{d}\Omega\mathrm{d}\omega}\right)_\mathrm{pm} = C_\mathrm{pm}\frac{k_\mathrm{f}}{k_\mathrm{i}} f_\mathrm{m}(\boldsymbol{Q})^2 \frac{\hbar\omega}{1-\exp(-\hbar\omega/k_\mathrm{B}T)}\chi(0) \times \frac{\kappa_1^2}{\kappa_1^2+q^2}\frac{\Gamma}{\Gamma^2+(\hbar\omega)^2}, \tag{2.6}$$

where C_pm is a scale factor. Note that, the empirical scattering function $S(\boldsymbol{Q},\omega)$ in eq. (2.4) is suitable for our analysis, since Γ and κ_1 have quite different characters between the localized system and itinerant system.[30]

Therefore, in order to analyze magnetic excitaions in the paramagmetic state, we examine the q and κ_1 dependence of the linewidth Γ by fitting with the double Lorentzian scattering function. These data are compared with those from other cubic ferromagnets and existing theories.

§3. Experimental Details

The procedure for crystal growth is as follows.[32] Polycrystals of CoS_2 were made of Co (99.99%) and S (99.999%) raw material powder by sintering in silica tubes. We grew single crystals by the method of chemical transport technique and the condition below was found to be appropriate.[18] The powder of CoS_2 with the weight of 0.5 ~ 1 g was seald into a silica tube of 1cm diameter and about 15 cm long, with Cl_2 gas of 0.4 atom in pressure. The tube was set in a heater-furnace with 780°C at the hot zone and 720°C at the cool zone during 2 weeks. The single crystals with metallic lustre were grown up to the volume of about $(5\ \mathrm{mm})^3$ and they show high symmetric cleavage surfaces. The specific resistivity $R_{293\,\mathrm{K}}/R_{4\mathrm{K}}$ was about 60. The de Haas-van Alphen effect was also observed under the condition of 13 Tesla and 30 mK.[33] The rough estimation on the effective mass of $3m_\mathrm{e}$ was comparable to $3 \sim 6m_\mathrm{e}$ from the electronic specific heat.[12,13,18] Because of the large neutron absorption of cobalt nuclei and the small magnetic moment less than $1\mu_\mathrm{B}$ in CoS_2, it is of great advantage to our neutron inelastic scattering experiments to use the large sample in volume. We aligned five single crystals of CoS_2 in an alminium can, in such a way that each [0 1 $\bar{1}$] crystal axis be set vertically. Rotating the sample about [0 1 $\bar{1}$] axis, (*hll*) reflections were measured. The total volume of 0.5 cc is greater than twice as that as Iizumi *et al.* utilized before[22] and made us feasible to accomplish our fruitful experiments below.

The neutron scattering experiments were carried out on the triple-axis Tohoku University polarization analzer neutron spectrometer (TOPAN) installed at JRR-3 in Tokai. Pyrolytic graphite (PG) reflection through the (002) plane was used for bent monochrometer and analyzer both. A PG filter was inserted in the neutron path to remove higher order contaminations. The sample can filled with He gas was set up in a variable temperature cryostat. The temperature was monitored by a Pt-Co resistance thermometer attached at the bottom of the

can.

Most of the measurements for spin-wave scattering below T_C were conducted with fixed initial or final energy (E_i or E_f) of about 15 or 30 meV,

and with horizontal collimation of 30′-60′-60′-100′. Taking account of the small magnetic anisotropy in CoS_2,[18,22,34,35] we investigated the magnon dispersion relation along [111] direction only in the first Brillouin zones with the center of $(1,1,1)$, $(1,-1,-1)$ or $(2,0,0)$ magnetic Bragg points.

The paramagnetic scattering measurements above T_C were conducted with E_i or E_f of about 15 meV and with horizontal collimation of 15′-100′-100′-100′. Energy spectra centered at zero energy transfer were detected around the $(1,-1,-1)$ magnetic reciprocal point. The elastic incoherent component was subtracted by making use of the spectra observed at any random positions at where no obstacles such as phonon scattering are expected.

The measured intensity $I(\boldsymbol{Q}_0,\omega_0)$ is given by the convolution of the cross-section with a resolution function of the spectrometer $R(\Delta\boldsymbol{Q},\Delta\omega)$;[36,37]

$$I(\boldsymbol{Q}_0\ ,\ \omega_0) = \int \frac{\hbar k_f}{m_N}\frac{d^2\sigma}{d\omega d\Omega}(\boldsymbol{Q},\omega)R(\boldsymbol{Q}-\boldsymbol{Q}_0,\omega-\omega_0)d\boldsymbol{Q}d\omega \propto \int \frac{k_f^2}{k_i}S(\boldsymbol{Q},\omega)R(\boldsymbol{Q}-\boldsymbol{Q}_0,\omega-\omega_0)d\boldsymbol{Q}d\omega. \quad (3.1)$$

Here, the Gaussian form is supposed for $R(\Delta\boldsymbol{Q},\Delta\omega)$. As for the magnetic form factor $f_m(\boldsymbol{Q})$ which appears in $S(\boldsymbol{Q},\omega)$, we use the calculated value for Co^{2+} free cation,[38] based on the experimental proof from polarized neutron diffraction measurements.[39] In our analysis, moreover, the monitor counts were corrected taking account of higher order neutrons[40] if necessary.

§4. Experimental Results and Analyses

4.1 $T < T_C$

Firstly, we describe the low-energy excitations mesured in the small (q,ω) region. Neutron groups of the spin-wave scattering detected below a momentum transfer of $q = 0.26$ Å^{-1} for ω-scans (constant-q) and below an energy transfer of $\hbar\omega = 7$ meV for q-scans (constant-E), are shown in Figs. 1(a) and 1(b), respectively. Three parameters C_{sw}, D and Γ for constant-q spectra, whereas two parameters C_{sw} and D for constant-E spectra in eq. (2.3) were determined by fitting the experimental data to the theoretical cross-section convoluted with the instrumental resolution. The determined energy and momentum of magnetic excitations immediately lead a dispersion relation, $\hbar\omega_q = (107 \pm 7)q^2$. The solid lines in Fig. 1(a) are drawn as the results from the fitting procedure, while in Fig. 1(b) the lines represent the calculated (not fitted) intensity holding three parameters fixed; $D = 107$ meVÅ^2, $\Gamma = 0.9$ meV and C_{sw} determined from the constant-E scan at the energy transfer of 4 meV. The scattering profiles at different temperatures, one well below T_C and the other above T_C, are typically shown in Fig. 2. It is obvious that collective excitations, or spin-wave like modes disappear

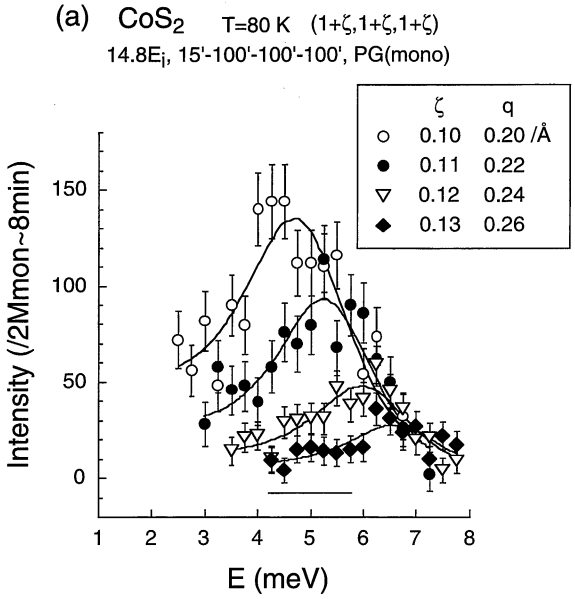

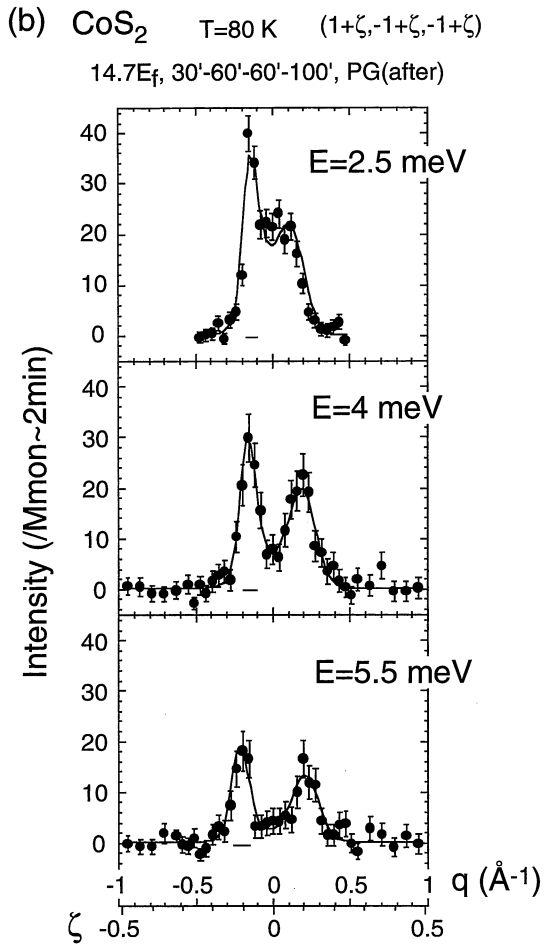

Fig. 1. Magnon groups at 80 K observed (a) around $(1,1,1)$ with constant-q mode, $14.8E_i$, PG filter before sample and horizontal collimation of 15′-100′-100′-100′; and (b) around $(1,-1,-1)$ with constant-E mode, $14.7E_f$, PG filter after sample and horizontal collimation of 30′-60′-60′-100′. By using eqs. (2.3) and (3.1), solid lines are (a) fitted with three parameters C_{sw}, D and Γ, whereas (b) calculated with fixed three values $C_{sw}(\hbar\omega = 4$ meV), $D = 107$ meVÅ^2 and $\Gamma = 0.9$ meV. Horizontal bars represent a measure of energy or q resolution at each condition.

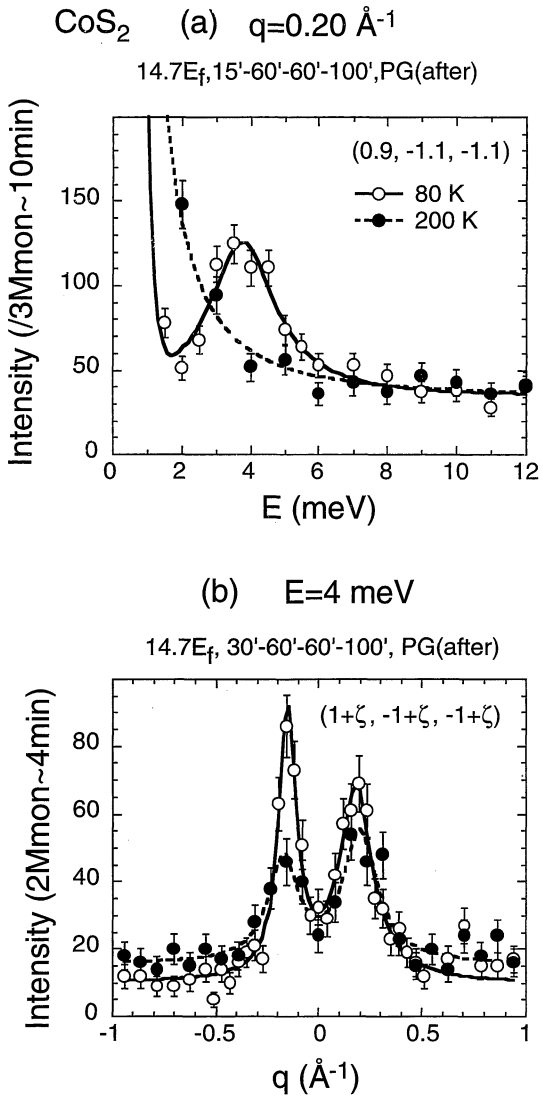

Fig. 2. Variations of spin-wave excitations with temperature across T_C. Constant-q peak sharply disappears in (a), whereas some components in the constant-E slice remain even above T_C (200 K = $1.65T_C$) in (b). Solid and broken lines are drawn as a guide to the eyes.

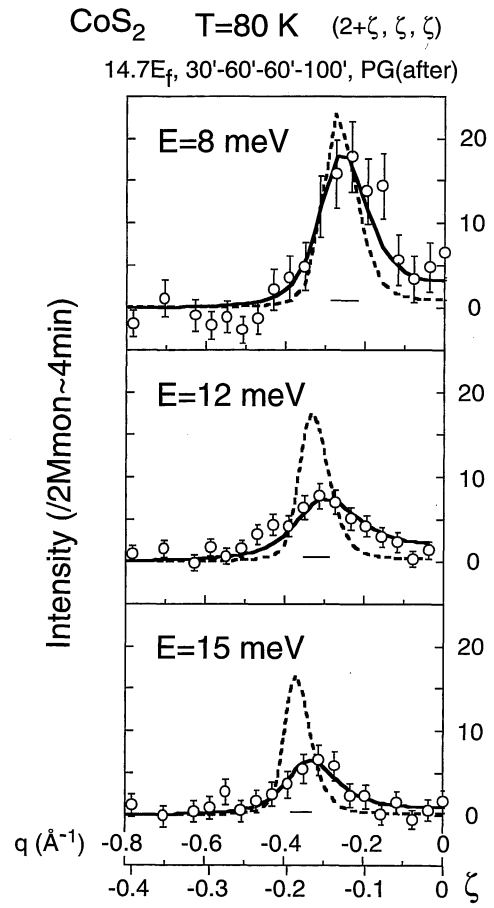

Fig. 3. Constant-E spectra at 80 K around $(2,0,0)$ for middle-energy excitations using the resolution of $14.7E_f$ with horizontal collimation 30′-60′-60′-100′. Focusing effects in the triple-axis spectrometer are expected at the indicated scanning side. By using eqs. (2.3) and (3.1), broken lines are just calculated with three fixed values [$C_{sw}(\hbar\omega = 4$ meV), D and Γ] deduced from the spin-wave excitation regime, while solid lines are fitted with two parameters C_{sw} and Γ holding $D = 107$ or 125 meVÅ^2. Horizontal bars represent a measure of q resolution at each energy transfer.

above T_C, though a pair of peaks still remains in the constant-E slice, which will be focused below in the next paramanetic scattering. As for the linewidth we obtained the nearly constant small value, $\Gamma = 0.9 \pm 0.2$ meV at 80 K. C_{sw} corresponding to the spin-wave scattering intensity[41] is almost constant below $q \leq 0.26$ Å^{-1} as shown later in Fig. 4(b). As a result, it is clear that the low-energy magnetic excitations in the small-q range are described by the normal spin-wave mode.

Next, we describe the middle-energy excitations beyond the typical spin-wave excitation regime. Due to the steep gradient of dispersion surface in the middle (q,ω) space, we performed only constant-E scans. The examples of q-spectra detected with the energy transfers of $8 \leq \hbar\omega < 19$ meV are displayed in Fig. 3. Following the low-energy scans, we calculated the scattered intensities with the constants D, Γ and C_{sw}(determined at $\hbar\omega =$ 4 meV) convoluted with the instrumental resolution and drew the results with broken lines in Fig. 3. The higher the spin-wave energy become, the more remarkable discrepancy we find between experiments and calculations. Then, we fitted the observed spectra to the calculated curves with two adjustable parameters C_{sw} and Γ and a fixed parameter of $D = 107$ and 125 meVÅ^2 for $\hbar\omega \leq 10$ and > 10 meV, respectively. The solid lines represent the fitted results, which give a reasonable agreement to the experimental points. Through the conversion of $\Delta q \rightarrow \Delta\hbar\omega$ based on the dispersion relation, we evaluated Γ from constant-E slices. Γ and C_{sw} plotted as a function of q, including the data from the spin-wave excitaion regime, are shown in Figs. 4(a) and 4(b), respectively. Note that C_{sw} is plotted on a normalized scale where the scattered intensities are adjusted so that the data points with $14.7E_f$ and $30.4E_f$ superpose at $\hbar\omega = 12$ meV. Although the experimental accuracy of Γ and C_{sw} is not excellent, the broadning of the magnetic excitaions becomes significant in $q \geq 0.27$ Å^{-1}. Therefore, magnetic excitations are regarded not as the simple spin-waves but the interacted spin-waves with other freedom. This consideration must be supported by the fact of a sudden drop in intensity in this q range. Since the twin peaked structure never disappears in the constant-

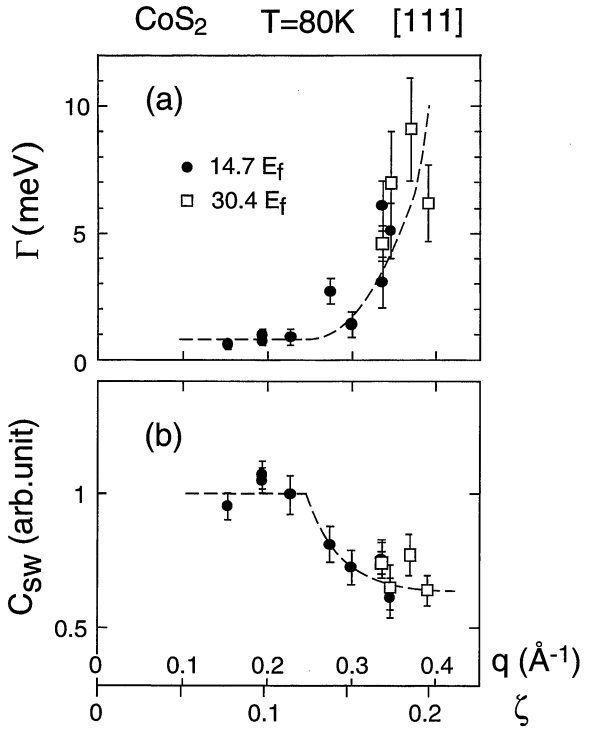

Fig. 4. Plots of (a) linewidth Γ as well as (b) scale factor $C_{\rm sw}$ against q, determined with two different conditions of $14.7E_{\rm f}$ and $30.4E_{\rm f}$. Broken lines are just drawn as a guide to the eyes.

E scans even at 200 K ($1.65T_{\rm C}$) as shown in Fig. 5, the excitations can't be defined as conventional spin-waves.

We now describe high-energy excitations. A series of q-scans detected above 19 meV are shown in Fig. 6. A weak but distinct ridge continues from the lower q region up to the momentum transfer of 0.5 Å^{-1} (halfway to the zone boundary along [111]), where the excitation energy reaches to 30 meV. After the similar fitting procedure to the one described above with the conversion of $\Delta q \rightarrow \Delta\hbar\omega$, the determined value of Γ becomes large as the comparative order of the excitation energies, but the ridge of intensity maxima shows a quadratic dispersion $\hbar\omega_q = 125q^2$ which extends from the middle-energy region. No distinct temperature variation was also observed in the temperature range observed. We will further discuss the origin of this excitation in the next section.

Finally, we mention the result from a series of energy scans measured with $30.4E_{\rm f}$ over a wide q range. We observed a broad weak ridge at around the energy transfer of 20 meV across the whole Brillouin zone. No changes were recognized above $T_{\rm C}$ in the energy spectra. Note that, the source of phonon scatering forming the ridge was proved to be impossible by the fact of the q- and temperature-dependence of the scattered intensities.

4.2 $T > T_C$

Energy scans searching magnetic scattering above $T_{\rm C}$ were made. The contribution of an incoherent elastic componet was experimentally deterrmined from the profiles measured at $(1.4, 1.4, 1.4)$ and $(1.9, -0.9, -0.9)$ positions. Some examples of the paramagnetic scattering corrected the background are demonstrated in

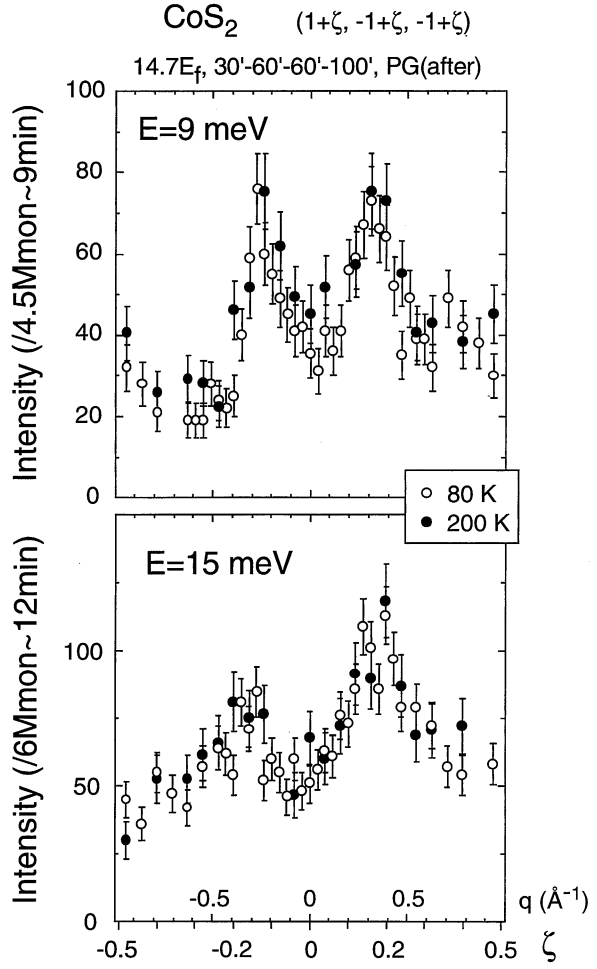

Fig. 5. Constant-E spectra for middle-energy excitations below (open circles) and above $T_{\rm C}$ (closed circles).

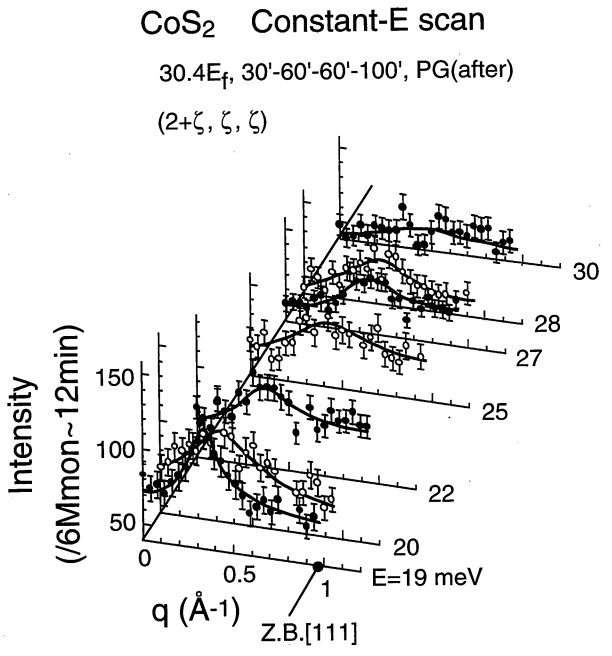

Fig. 6. Series of constant-E spectra at 80 K around $(2, 0, 0)$ for high-energy excitations using the resolution of $30.4E_{\rm f}$ with a PG filter after sample and the horizontal collimation of 30′-60′-60′-100′. Solid lines are drawn as a guide to the eyes.

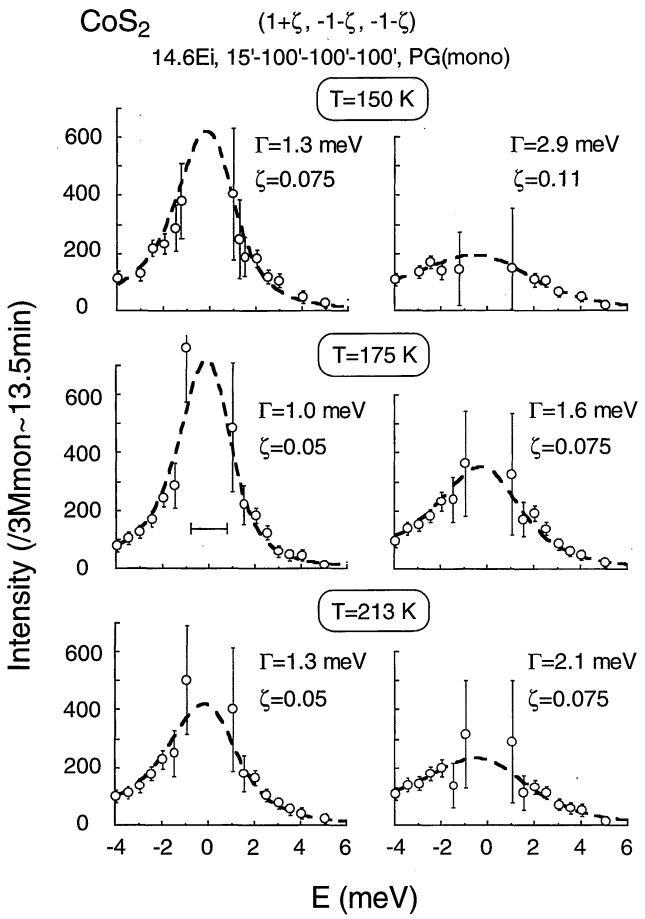

Fig. 7. Paramagnetic scattering profiles measured at various ζ (or q) and T around $(1,-1,-1)$ using $14.6E_i$ with a PG filter before sample and the horizontal collimation of 15′-100′-100′-100′. Incoherent elastic components were subtracted as described in the text. Broken lines are calculated by eq. (2.6) convoluted with the instrumental resolution [eq. (3.1)].

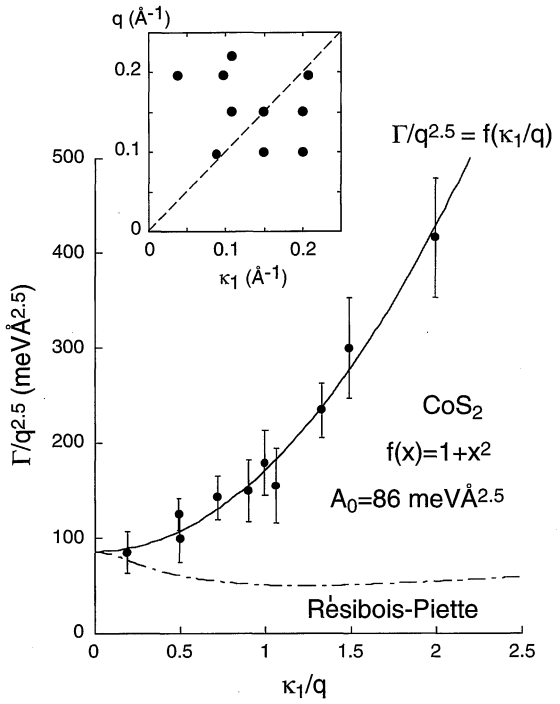

Fig. 8. Scaling of linewidth. $\Gamma/q^{2.5}$ is plotted against κ_1/q. Solid line represents the dynamical scaling law [eq. (2.5)] with $f(x) = 1 + x^2$ and $A_0 = 86$ meVÅ$^{2.5}$, while chain line expresses the Résibois-Piette function normalized at $\kappa_1/q = 0$. The inset shows the measured points in $\kappa_1 - q$ plane in which broken line indicates $\kappa_1 = q$.

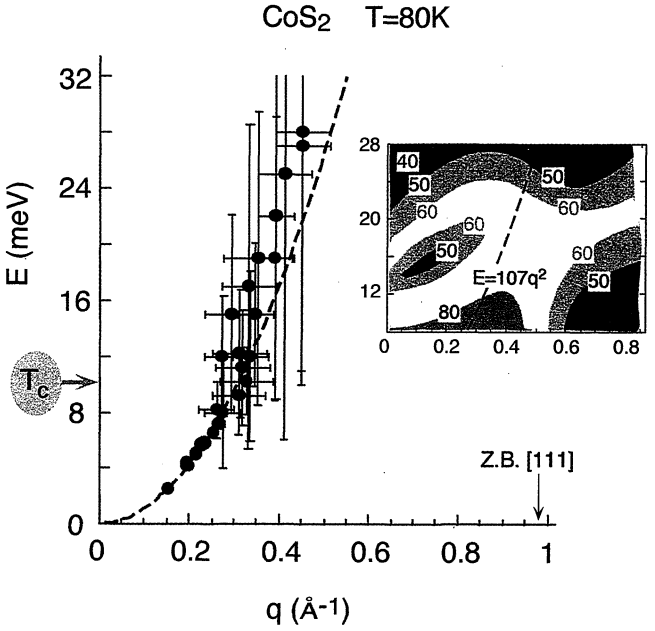

Fig. 9. Dispersion relation in CoS_2 at 80 K along [111] direction. Each vertical bar represents the magnitude of Γ. Broken line is calculated by $E = 107q^2$, which is determined in the low q region. The inset shows the contour map measured with constant-q mode using $30.4E_f$ with horizontal collimation 30′-60′-60′-100′ and PG (after sample) during $4M$ monitor time (~8 min).

Fig. 7. Broken lines were calculated by the paramagnetic scattering cross-section in eq. (2.6) convoluted with the instrumental resolution. Assuming the dynamical scaling law predicted in eq. (2.5), the data of $\Gamma/q^{2.5}$ or $A_0 f(\kappa_1/q)$ are plotted against κ_1/q in Fig. 8, where the inverse correlation length κ_1 was calculated by the experimentally determined result of $\kappa_1(T) = 0.232\,(T/121.0-1)^{0.54}$ Å^{-1} [18] Data points taken at different temperatures and wave-vectors fall on a single curve as shown in Fig. 8. The inset indicates that the q and κ_1 are individually chosen for each scan. The scaling function of $f(x)$ is quite different from the Résibois-Piette function,[42] but the experimental results are well fitted to $\Gamma = A_0 q^{2.5}[1 + (\kappa_1/q)^2]$; i.e. $f(x)$ becomes a good approximaiton of $(1+x^2)$, like the case of MnSi.[30] The fit gives $A_0 = 86 \pm 2$ meVÅ$^{2.5}$.

§5. Discussion

5.1 *Spin dynamics in ferromagnetic state*

The energy dispersion relation as well as the linewidth representing magnetic excitations at low temperatures are summurized in Fig. 9. The vertical bar on each data point represents *not* the error for the determination of maximum in intensity *but* the magnitude of Γ. The broad peak observed in energy spectra at around 20 meV is presented in the inset as a contour plot.

One of the characteristic feature is that at $q \approx 0.27$ Å^{-1}, Γ increases discontinuously and the dispersion relation deviates upward from the q^2-relation determined

in the spin-wave excitaion range as depicted with a broken line. It should be noted here that the transition energy ($\approx$ 8 meV) corresponds to the ferromagnetic ordering temperature T_C of CoS_2. Hence, we speculate that a Stoner boundary locates at $(q,\omega) \approx (0.27\ \text{Å}^{-1}, 8\ \text{meV})$ along [111] direction, above which spin-waves become overdamped. As a matter of fact, we confirmed the decrease in the spin-wave intensities as q increased [Fig. 4(b)], suggesting that collective excitations merge into the Stoner continuum. This fact is also consistent with that the constant-E spectra are similar below and above T_C above the Stoner boundary (Fig. 5), which suggests the temperature insensitive character of Stoner excitations.

The existence of Stoner excitations were reported by the Oak Ridge group[43-45] for other ferromagnetic metals, Fe and Ni which are categorized to be in the medium electron correlation system. As far as we know, the systematic study on Stoner excitations has been performed only for the itinerant ferromagnet MnSi by Ishikawa and his co-workers.[46] In this case neutron scattering was made under the external fields. They pointed out not only a gradual decrease of spin-wave scattering intensities but also a deviation of the dispersion curve from a q^2-relation. Furthermore, an increase of the linewidth started near the Stoner boundary, corresponding to the energy of T_C in MnSi. A fairly good agreement was also obtained between the experimental contour lines and calculated contour maps based on the simple RPA for electron gas. The essential part is that like present study the magnetic excitations below the Stoner boundary are temperature-dependent (well defined spin-waves below T_C and overdamped responses at near T_C), and that the broad signature above this boundary is insensitive to temperature.

Although theoretical calculations on the $\text{Im}\chi(\boldsymbol{Q},\omega)$ for CoS_2 are not available, we speculate the existence of Stoner excitations in CoS_2, since the experimental results are qualitatively the same as MnSi.

There are quantitative differences on between CoS_2 and MnSi data. One is the upward deviation of dispersion relation above the Stoner boundary in CoS_2, in contrast with the small downward shift occured at near the Stoner boundary in MnSi. One possible explanation to reconcile this difference is that spin-wave like excitations may hybridize with the broad ridge peaked at around 20 meV which seems to be an optical branch. The other difference is a sharp increase of Γ in CoS_2, which is consistent with the stronger hybridization between spin-wave mode and Stoner continuum. This unique aspect must be studied theoretically and the theoretical calculations for $\text{Im}\chi(\boldsymbol{Q},\omega)$ based on the realistic band structure of CoS_2 are strongly desired.

5.2 *Spin dynamics in paramagnetic state*

$S(\boldsymbol{Q},\omega)$ in the paramagnetic state can be calculated with $\Gamma = 86q^{2.5}[1+(\kappa_1/q)^2]$, $\kappa_1 = 0.232(T/121.0-1)^{0.54}$ and $\chi_0 = (T-121.0)^{-1.16}$ in eq. (2.4). The calculated contour map for the simple paramagnetic scattering function is presented in Fig. 10(a) with relative numerical values. As expected easily from the Fig. 10(a),

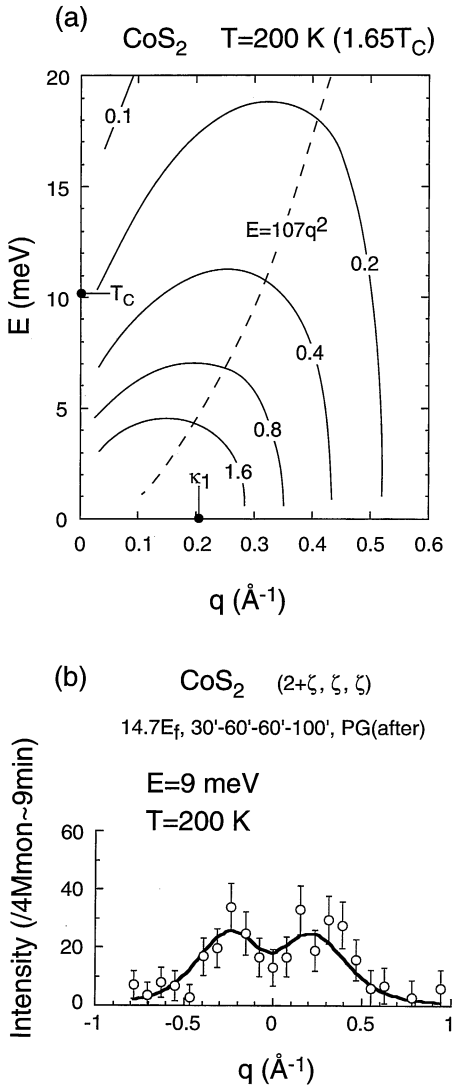

Fig. 10. (a) Calculated contour map for the simple paramagnetic scattering function [eq. (2.4)] at 200 K with relative numerical values. The used parameters are given in text. Broken line $E = 107q^2$ represents the spin-wave dispersion curve at $T = 0.7T_C$. (b) Reproduction of constant-E slice at 200 K. Solid line is calculated by using eqs. (2.6) and (3.1) with parameters given in text.

we can also reproduce the constant-E peaks as shown in Fig. 10(b) where the instrumental resolution effect is convoluted. It is important that the paramagnetic scattering of the double Lorentzian $S(\boldsymbol{Q},\omega)$ shows remarkable peaks in constant-E scans but no peaks in constant-q scans, like we find here. This feature was completely understood by the extensive works at Brookhaven for Fe,[25] Ni,[26] Pd_2MnSn[28] and MnSi.[29,30] The temperature insensitive peaks observed in constant-E scans (Figs. 5 and 6) are also understandable with the concept of the paramagnetic scattering in a metallic ferromagnet.

Let us evaluate the itinerancy of magentic electrons from the paramagnetic scattering by making use of the parameter A_0[28] in various cubic ferromagnets. A_0 or in reduced wave-vector units A_0^*, and T_C are widely spread in each material as shown in Table I. However, if A_0^* is properly scaled by T_C, we find that $A_0^*/T_C \simeq 1$ for EuO and Pd_2MnSn (localized system) whereas $A_0^*/T_C \gg 1$ for

Table I. Dynamical magnetic parameters for cubic ferromagnets. A_0^* and κ_0^* respectively correspond to A_0 and κ_0 expressed in units of reduced wave-number of the inverse plane distance d along [110] for Fe and MnSi, and [111] for others. $\hbar\omega_q = Dq^2$, $\Gamma = A_0 q^{2.5}$ at T_C and $\kappa_1 = \kappa_0(T/T_C - 1)^\nu$. $\nu = 0.5$ for MnSi, 0.54 for CoS_2 and 0.7 for others. D values at $T = 0.8T_C$ are listed except CoS_2 for $0.7T_C$.

	T_C (K)	d (Å^{-1})	D (meVÅ^2)	κ_0^*	A_0 (meVÅ$^{2.5}$)	A_0^* (meV)	A_0^*/T_C (meVK^{-1})
EuO	69	2.1	7.4	0.30	8.3	53	0.77
Pd_2MnSn	190	1.7	70	0.22	60	230	1.2
Fe	1040	3.1	175	0.34	140	2400	2.3
MnSi	30	1.9	50	0.09	20	100	3.3
CoS_2	121	2.0	107	0.12	86	460	3.8
Ni	631	3.1	330	0.20	350	5900	9.4

others. The ratio A_0^*/T_C may be used as a measure for the itinerancy of electrons. The value for CoS_2 suggests the non-localized spin character of magnetic electrons.

§6. Conclusion

Neutron inelastic scattering experiments well below T_C have revealed that two types of magnetic excitations exist in CoS_2. One is the normal spin-wave excitations following a q-quadratic relation in small (q, ω) region. The other is the broad and the temperature independent excitations extending up to halfway to the zone boundary and up to the energy of $3k_BT_C$. We assign it as the Stoner excitaions where lower energy boundary corresponds to the T_C of CoS_2.

The experiments above T_C have shown the validity of a simple paramagnetic scattering function of the double-Lorentzian with respect to q and ω. The analyses of $\mathrm{Im}\chi(\boldsymbol{Q}, \omega)$, in particular the q- and κ_1-dependence, also indicate that the itinerancy in CoS_2 is quite similar to the itinerant ferromagnet MnSi.

In conclusion, the spin dynamics observed in both ferromagnetic and paramagnetic states provides a clear evidence of the characteristics in the itinerancy of magnetic electrons, though the static properties put CoS_2 in the intermediate class.

Theoretical calculations of the dynamical magnetic susceptibility $\chi(\boldsymbol{Q}, \omega)$ based on a realistic band structure for CoS_2 are highly desirable to interprete the dynamical responces presented here; namely the spin-wave like dispersion relation, the Stoner excitations, the magnetic ridge peaked at around 20 meV and $\mathrm{Im}\chi(\boldsymbol{Q}, \omega)$ above T_C etc.

Acknowledgements

The authors would like to thank Professors T. Suzuki, T. Komatsubara, Y. Kuramoto and Y. Yamaguchi for their valuable discussions. We also thank Drs. M. Takeda and K. Hirota for their helpful technical advices on neutron inelastic scattering experiments, Mr. M. Onodera for his technical assistance in single crystal growth and Mr. K. Nemoto for his assistance in neutron scattering experiments on TOPAN. The work has been supported under the Grant in Aid for the Science Research by the Ministry of Education, Science, Sports and Culture.

1) H. S. Jarrett, W. H. Cloud, R. J. Bouchard, S. R. Butler, C. G. Frederick and J. L. Gillson: Phys. Rev. Lett. **21** (1968) 617.
2) K. Adachi, K. Sato and M. Takeda: J. Phys. Soc. Jpn. **26** (1969) 631; *ibid.* 639.
3) J. A. Wilson: *The Metallic and Non-Metallic States of Matter*, ed. P. P. Edwards and C. R. N. Rao (Taylor & Francis, London, 1985) p.215.
4) T. A. Bither, P. C. Donohue, W. H. Cloud, P. E. Bierstedt and H. S. Young: J. Solid State Chem. **1** (1970) 526.
5) K. Adachi, M. Matsui and M. Kawai: J. Phys. Soc. Jpn. **46** (1979) 1474.
6) K. Adachi, M. Matsui, Y. Omata, H. Mollymoto, M. Motokawa and M. Date: J. Phys. Soc. Jpn. **47** (1979) 675.
7) S. Ogawa, S. Waki and T. Teranishi: Int. J. Magn. **5** (1974) 349.
8) S. Ogawa: J. Appl. Phys. **50** (1979) 2308.
9) D. W. Bullett: J. Phys. C **15** (1982) 6163.
10) A. Ohsawa, H. Yamamoto and Y. Watanabe: J. Phys. Soc. Jpn. **37** (1974) 568.
11) K. Sato: J. Phys. Soc. Jpn. **53** (1984) 1617.
12) S. Ogawa and T. Yamadaya: Phys. Lett. **47A** (1974) 213.
13) S. Waki and S. Ogawa: J. Phys. Soc. Jpn. **32** (1972) 284.
14) N. Kasai: J. Phys. Soc. Jpn. **35** (1973) 1552.
15) See review article by T. Moriya: *Spin Fluctuations in Itinerant Electron Magnetism* (Springer-Verlag, Berlin, Heidelberg, New York, Tokyo, 1985).
16) T. Moriya and Y. Takahashi: J. Phys. Soc. Jpn. **45** (1978) 397.
17) Y. Takahashi and M. Tano: J. Phys. Soc. Jpn. **51** (1982) 1792.
18) H. Hiraka and Y. Endoh: J. Phys. Soc. Jpn. **63** (1994) 4573.
19) H. Hiraka and Y. Endoh: J. Phys. Soc. Jpn. **65** (1996) 3740.
20) S. Yomo: J. Phys. Soc. Jpn. **47** (1979) 1486.
21) K. Makoshi and T. Moriya: J. Phys. Soc. Jpn. **38** (1973) 10.
22) M. Iizumi, J. W. Lynn, A. Ohsawa and H. Itoh: AIP Conf. Proc. **29** (1977) 4956.
23) T. Izuyama, D. J. Kim and R. Kubo: J. Phys. Soc. Jpn. **18** (1963) 1025.
24) W. Marshall and S. W. Lovesey: *Theory of Thermal Neutron Scattering* (Oxford U. P., London, 1971).
25) J. P. Wicksted, P. Böni and G. Shirane: Phys. Rev. B **30** (1984) 3655.
26) O. Steinsvoll, C. F. Majkrzak, G. Shirane and J. Wicksted: Phys. Rev. B **30** (1984) 2377.
27) P. Böni and G. Shirane: Phys. Rev. B **33** (1986) 3012.
28) G. Shirane, Y. J. Uemura, J. P. Wicksted, Y. Endoh and Y. Ishikawa: Phys. Rev. B **31** (1985) 1227.
29) Y. Ishikawa, Y. Noda, C. Fincher and G. Shirane: Phys. Rev. B **25** (1982) 254.
30) Y. Ishikawa, Y. Noda, Y. J. Uemura, C. F. Majkrzak and G. Shirane: Phys. Rev. B **31** (1985) 5884.
31) B. I. Halperin and P. C. Hohenberg: Phys. Rev. B **177** (1969) 952.
32) R. J. Bouchard: J. Cryst. Growth **2** (1968) 40.
33) A. Ishiguro: private communication.
34) K. Adachi, K. Sato, M. Okimori, G. Yamauchi, H. Yasuoka and Y. Nakamura: J. Phys. Soc. Jpn. **38** (1975) 81.
35) T. Sekiguchi, T. Miyadai and K. Manabe: J. Magn. Magn.

Mater. **28** (1982) 154.
36) M. J. Cooper and R. Nathans: Acta Crystallogy. **23** (1967) 357.
37) N. J. Chesser and J. D. Axe: Acta. Crystallogy. Sect. A **29** (1973) 160.
38) R. E. Watson and A. J. Freeman: Acta Crystallogy. **14** (1961) 27.
39) A. Ohsawa, Y. Yamaguchi, H. Watanabe and H. Itoh: J. Phys. Soc. Jpn. **40** (1976) 986.
40) R. A. Cowley, G. Shirane, R. J. Birgeneau and H. J. Guggenheim: Phys. Rev. B **15** (1977) 4292.
41) E. D. Thompson: Phys. Rev. Lett. **19** (1967) 635.
42) P. Résibois and C. Piette: Phys. Rev. Lett. **24** (1970) 514.
43) H. A. Mook and M. Nicklow: Phys. Rev. B **7** (1972) 336.
44) J. W. Lynn: Phys. Rev. B **11** (1975) 2624.
45) H. A. Mook, R. M. Nicklow, E. D. Thompson and M. K. Willkinson: J. Appl. Phys. **40** (1969) 1450.
46) Y. Ishikawa, G. Shirane, J. A. Tarvin and M. Kohgi: Phys. Rev. B **16** (1977) 4956.